JOURNAL OF APPLIED ELECTROCHEMISTRY **26** (1996) 1225–1234

Pulse plating of Zn–Ni alloy coatings

A. M. ALFANTAZI*§, J. PAGE‡, U. ERB*

Department of Materials and Metallurgical Engineering and Department of Chemistry‡, Queen's University, Kingston, Ontario, Canada K7L 3N6*

Received 1 August 1995; revised 16 March 1996

In this work the electrodeposition of Zn–Ni alloy coatings from a chloride-based electrolyte using a square-wave current pulse-plating technique was investigated. The effects of the pulse plating variables (peak current density, on-time and off-time) and some important bath conditions ($ZnCl_2$ and $NiCl_2.6H_2O$ concentrations in the bath as well as bath temperature) on the chemical composition, surface morphology, grain size, phase distribution and preferred orientation of the deposits were studied. The bath temperature had a very strong effect on the composition of the deposits which, in turn, had very strong effects on the phases present, surface morphology and grain size. The peak current density was found to have little effect on the composition and phases present, but had considerable effect on grain size. The on-time and off-time had no significant influence on the characteristics of the deposits, except for slight grain refinement observed with increasing off-time. Only the η, γ and α crystal phases were found in the deposits while other intermediate phases such as β and δ were not found in any of the deposits produced in this work. Grain refinement of the deposits down to the nanocrystalline range can be achieved by increasing the Ni content of the deposits.

1. Introduction

Presently, the most widely used corrosion protective coating for steel is zinc which is applied either by hot-dipping or electroplating processes. However, to achieve the desired levels of corrosion protection, the zinc coating must be thick enough (typically up to 25 μm) to endure the corrosive environment. The major disadvantages of using thick coatings are the poor formability and weldability [1]. Also, a thick coating makes it difficult to achieve a specular finish after painting [2]. This has led to the development of thinner electrodeposited coatings with improved properties compared with zinc. Alloys of zinc with the metals of the 8th-group (iron, nickel, cobalt, etc.) have been considered as prime candidates for this purpose. In particular, studies have shown that the corrosion resistance of electrodeposited Zn–Ni alloy coatings within a certain composition range (12–14 wt % Ni) can be 5–6 times better than for pure zinc of equal thickness [1, 3]. It has been further shown that the formability [4] and weldability [5] of Zn–Ni alloy coated steel are good.

Although Zn–Ni alloy electrodeposits are mainly used as coatings to improve the corrosion resistance of automobile steel bodies, these coatings have been considered for several other applications such as electrocatalytic water electrolysis [6, 7], coating for steel cord reinforcement of tires [8] and in the electronics industry [9]. Zn–Ni alloys have also been considered as alternative coatings to cadmium [10, 11]. Cadmium is a very poisonous metal and due to health hazards and risk of pollution, environmental regulations are encouraging the use of alternative protection systems. In one study, Zn–Ni alloys were plasma-sprayed at the interface of plasma-sprayed ceramic coatings on steel substrate to improve the corrosion and adhesion properties of the ceramic coating [12].

Pulse plating, with its several plating variables and higher peak current density compared to direct current (d.c.) plating, has received considerable interest [13] over the past 20 years and proved to be a viable route for materials processing [14]. Compared with d.c. electrodeposition, pulse plating can improve the deposition process and some deposit properties namely, porosity, ductility, hardness and surface roughness. Moreover for alloy codeposition, pulse plating can produce compositions and structures which are not obtainable with d.c. plating [13]. For many systems, the plating rate which is determined by the current density and current efficiency is normally higher in pulse plating than in d.c. plating. The higher the value of these two factors the greater the plating rate. For Zn–Ni, the current density typically used in d.c. plating ranges between 0.01 to 0.06 A cm^{-2} (100 to 600 A m^{-2}), although higher values were considered (up to 7000 A m^{-2}), while the average current density in pulse plating is much higher; in this present investigation, for instance, a range of 0.3 to 1.1 A cm^{-2} was studied. The other factor, current efficiency, typically ranges from 70 to 95% for d.c. plating and over 50% in pulse plating, depending on the plating conditions. It is therefore apparent that the higher plating rates obtainable

§ Author to whom correspondence should be addressed. Present address: Department of Metals and Materials Engineering, The University of British Columbia, Vancouver, BC, Canada, V6T 1Z4.

0021-891X

with pulse plating are mainly brought about by the relatively very high average current densities while maintaining a comparable current efficiency.

Although there is a large volume of literature available on the electrodeposition of Zn–Ni alloys [3], very little attention has been given to the pulse plating of these materials. In fact, only two papers [15, 16] have previously dealt with the pulse plating aspects of the Zn–Ni system. However, in both studies an ammonium chloride based electrolytes were used and the concentration of zinc in the electrolyte was low (2–10 g dm^{-3}). The electrolyte used in the present work is of different composition, containing no ammonium chloride but relatively high amounts of zinc (50 to 300 g dm^{-3}).

The objective of the present work is to study the pulse-plating of Zn–Ni alloy from a chloride based electrolyte. In particular, the influence of the pulse-plating parameters (on-time, off-time and peak current density), temperature and bath composition on the deposit microstructure, chemical composition and phases present were studied.

2. Experimental details

2.1. *Pulse electrodeposition of Zn–Ni alloys*

Using the information in the literature concerning the pulse plating of Zn–Ni alloys, preliminary work using the pulse plating technique was initiated. The starting values for the pulse plating variables, peak current density, on-time and off-time, were selected based on the work of Nenov *et al.* [15] since this is the only pulse plating study that reported the values of the pulse plating parameters for the Zn–Ni system.

An extensive pulse plating programme to study the effects of the plating variables on the deposition process and deposit characteristics was then set up using the optimum conditions and parameters ranges that were established in the preliminary pulse plating experiments. The final electrolyte composition and the bath conditions as well as the pulse plating parameters that were used in this work are shown in Table 1. The chloride based electrolyte having the composition shown in Table 1 was prepared by adding the appropriate amounts of $ZnCl_2$, $NiCl_2.6H_2O$, SLS (sodium lauryl sulfate, $NaC_{12}H_{25}SO_4$) and boric acid (H_3BO_3) to cold distilled water. SLS was used as a wetting agent to reduce risk of pitting. This particular wetting agent was chosen because it is widely used in industry. The boric acid was used to maintain the bath pH. The advantage of employing a high metal content (200 g dm^{-3}) is that higher current densities can be used and thicker deposits can be produced [17].

Table 1. Bath conditions and pulse plating parameters with their various ranges for Zn–Ni plating

Variable	*Range*
$ZnCl_2$	50–300 g dm^{-3}
$NiCl_2.6H_2O$	50–300 g dm^{-3}
H_3BO_3	40 g dm^{-3}
SLS	0.1 g dm^{-3}
Temperature	25–80 °C
pH	3.4 ± 0.1
Peak current density, I_p	1–3.6 A cm^{-2}
On-time, T_{on}	0.2–1.0 ms
Off-time, T_{off}	2.0–5.25 ms
Duty cycle, θ	3.5–33.0%
Frequency, f	160–450 Hz

Pulse plating of pure Zn and Zn–Ni alloys was carried out galvanostatically using cathodic square wave pulses. All deposits were produced using a Pulsestar pulse generator which can supply peak current densities of up to 25 A cm^{-2}.

A high purity (99.99%) nickel sheet (4 cm × 4 cm) contained in a titanium mesh basket was used as a soluble anode and its surface area was greater than that of the cathode (4:1 ratio) to ensure that there were no problems arising from anode polarization, particularly at high plating current densities. Commercial purity cold rolled copper sheets having exposed areas of 4 cm^{-2} were used as cathodes. The anode to cathode distance was maintained at about 2.5 cm. Before plating the cathode substrates were mechanically polished down to 600 grid SiC paper using standard metallographic techniques but the cathodes were not chemically pretreated.

The pH of the solution was monitored, but not adjusted, during the experiments. Between experiments, however, adjustments were made by the addition of hydrochloric acid (to lower pH) or ammonia (to increase pH). The experiments were conducted without stirring or agitation.

The experimental setup consisted of a standard two litre plating cell containing the electrolyte immersed in a temperature controlled water bath. The waveform of the pulsed current was periodically monitored on a storage oscilloscope.

After plating, the deposits were immediately rinsed in running tap water, dried with hot air and then subjected to further characterization.

The electrodeposition experiments were carried out by varying one parameter (in Table 1) at the time, with all other parameters being fixed at standard conditions. These standard conditions were chosen based on the literature review as well as the exploratory electrodeposition experiments and are given in Table 2. The reproducibility of the plating experiments was established by repeating most of the tests at least three times. The effect of the pulse plating parameters namely the on-time, off-time and peak current density as well as other bath conditions namely temperature, $ZnCl_2$ and $NiCl_2.6H_2O$ concentrations on the deposit characteristics were studied in the ranges shown in Table 1.

For comparison, a number of pure Zn electrodeposits were also produced by the pulse plating technique from a chloride based electrolyte which contained 200 g dm^{-3} $ZnCl_2$ and 40 g dm^{-3} H_3BO_3. Other plating conditions for the pure zinc are shown in Table 3.

Table 2. Standard conditions for pulse plating of Zn–Ni alloys

Parameter	*Value*
$ZnCl_2$	200 g dm^{-3}
$NiCl_2.6H_2O$	200 g dm^{-3}
H_2BO_3	40 g dm^{-3}
$NaC_{12}H_{25}SO_4$ (SLS)	0.1 g dm^{-3}
Temperature	40 °C
Peak current density, I_p	3.0 A cm^{-2}
On-time, T_{on}	0.25 ms
Off-time, T_{off}	4.75 ms
Duty cycle, θ	5%
Frequency, f	200 Hz
pH	3.40 ± 0.1

Table 3. Pulse plating parameters for pure Zn coatings

Parameter	*Value*
Peak current density, I_p	3.0 A cm^{-2}
On-time, T_{on}	0.25 ms
Off-time, T_{off}	4.75 ms
Duty cycle, θ	5.0%
Frequency, f	200 Hz
Temperature	65 °C
pH	3.80 ± 0.1
Anode	titanium

2.2. *Microstructural studies*

The Zn and Zn–Ni alloys electrodeposits produced in this work were characterized for their surface morphology, chemical composition as well as microstructure (grain size, phases present and preferred orientation). The surface morphology of most deposits and the grain size for deposits with relatively large grain size (> 300 nm) were studied by scanning electron microscopy (SEM) using a Jeol JSM-840 SEM operated at 20 kV. The chemical composition of the electrodeposits was determined using the TN5500 energy dispersive X-ray spectroscopy (EDS) system attached to the SEM. All chemical composition values given in the following sections are quoted in weight percent and represent the average of at least five measurements. X-ray diffraction (XRD) was used to determine the phases present and the preferred orientation of the deposits. A Rigaku Miniflex X-ray diffractometer with a CuK_α radiation ($\lambda = 0.15418$ nm) was employed to obtain XRD spectrums using standard θ–2θ geometry. A manual search and match using the JCPDS powder diffraction file cards was used for phase identification. For deposits with nanocrystalline structure, XRD was also used to determine the grain size. The grain size measurements for the nano-structured deposits were based on the Scherrer line broadening equation, which is well suited to detect grain diameters less than 100 nm [18].

3. Results and discussion

3.1. *Effect of bath composition*

It is very important to optimize the concentrations of the different metal ions in the plating solution, especially when developing an industrial alloy plating process such as Zn–Ni. The effect of the bath composition was studied by varying (i) the $ZnCl_2$ concentration, and (ii) the $NiCl_2.6H_2O$ concentration. These series of experiments were carried out using the standard conditions outlined in Table 2 except for the variable being tested.

3.1.1. $ZnCl_2$ concentration. $ZnCl_2$ concentrations in the range of 50 to 300 g dm^{-3} were considered while maintaining the $NiCl_2.6H_2O$ content in the bath at 200 g dm^{-3}. Figure 1 shows the effect of varying the $ZnCl_2$ concentration on the chemical composition of the deposit (nickel content in wt %). As expected, higher $ZnCl_2$ concentrations in the bath gave initially higher zinc content in the deposit (lower Ni content). However at $ZnCl_2$ concentrations above approximately 150 g dm^{-3}, the alloy composition became almost independent of further increases in the $ZnCl_2$ concentration in the bath. The results indicate that the electrodeposition under these plating conditions is of the anomalous type over the entire range of $ZnCl_2$ concentration as described by Brenner [17]. As shown in Table 4, the percentage of the more noble metal (Ni) in the deposit is much less than in the bath. The variation of the percentage of Ni ions in the bath from 68 to 26.5%

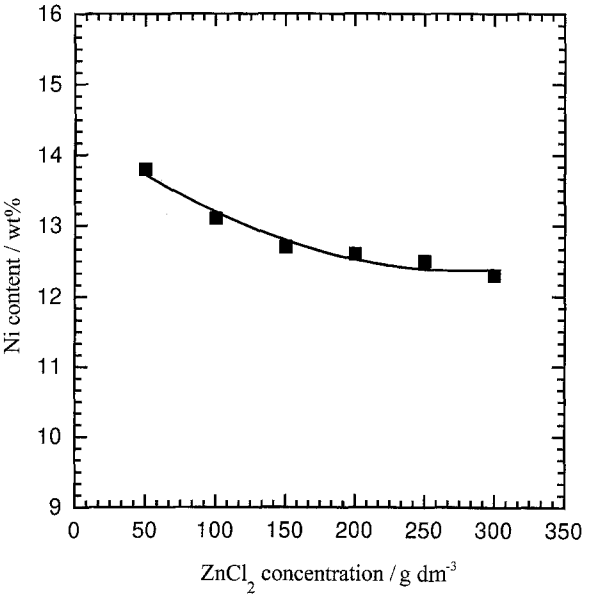

Fig. 1. Change in deposit Ni content as a function of $ZnCl_2$ concentration in the bath.

Table 4. Ni content in bath and deposit as a function of $ZnCl_2$ concentration in the bath

$ZnCl_2$/g dm^{-3}	*Ni in bath*/wt %	*Ni in deposit*/wt %
50	68.0	14.00
100	52.0	13.25
150	47.0	12.75
200	35.0	12.50
250	30.0	12.40
300	26.5	12.25

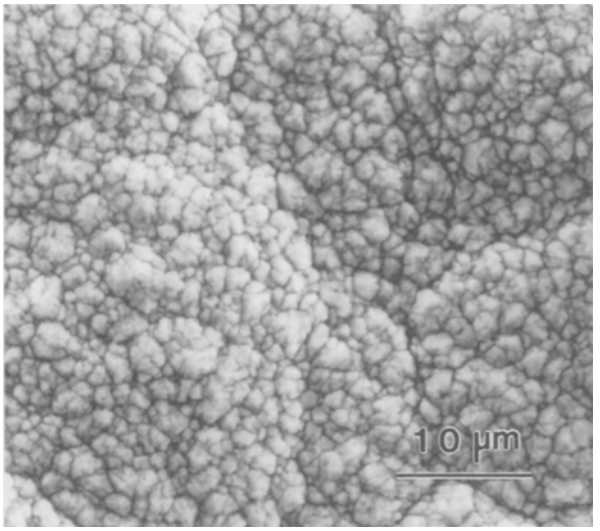

Fig. 2. SEM micrographs of pulse plated Zn–Ni alloy electrodeposits produced at $ZnCl_2$ concentrations of 300 g dm^{-3}.

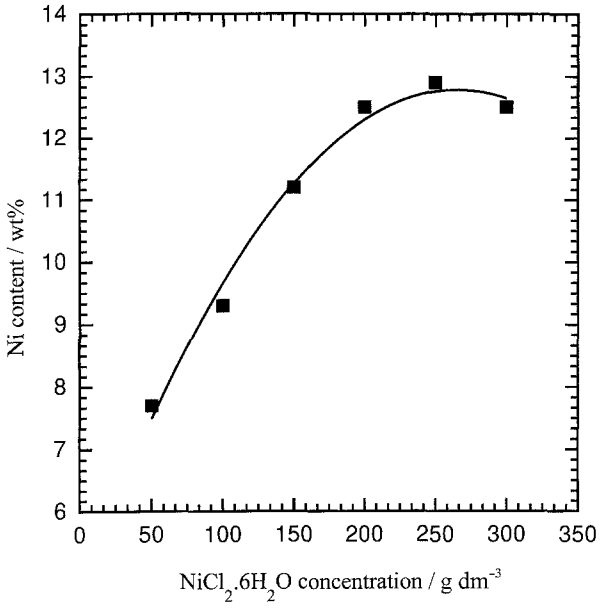

Fig. 3. Change in deposit Ni content as a function of $NiCl_2.6H_2O$ concentration in the bath.

Table 5. Ni content in bath and deposit as a function of $NiCl_2.6H_2O$ concentration

$NiCl_2.6H_2O$/g dm^{-3}	*Ni in bath*/wt %	*Ni in deposit*/wt %
50	12.0	7.7
100	21.3	9.5
150	28.9	11.2
200	35.5	12.5
250	40.4	12.7
300	44.8	12.5

(Table 4), which was calculated using the ratio of Ni/(Zn + Ni) in the bath was brought about simply by varying the zinc content of the bath ($ZnCl_2$ additions) while fixing the nickel content in the bath. Using different electrolytes and d.c. plating conditions a number of previous investigators observed similar trends [19–21].

The surface morphology of the electrodeposits was not significantly influenced by the change in $ZnCl_2$ concentration in the range tested. As a typical example, a SEM micrograph for Zn–Ni alloy coating produced at $ZnCl_2$ concentrations of 300 g dm^{-3} is shown in Fig. 2. The deposits have a fine-grained structure with grain size of about 0.5 to 2 μm. These results were expected since the chemical composition of the deposit did not change significantly. It has been shown previously that the nickel content in the deposit is the major parameter controlling the morphology in pulse-plated Zn–Ni alloys [22]. All deposits have the γ single phase structure as determined by XRD analysis.

Based on the above results it can be concluded that the desired chemical compositions (12–14 wt % Ni) for corrosion protection are obtained within the entire range of $ZnCl_2$. However, the high $ZnCl_2$ concentration (200 g dm^{-3}) were chosen for the subsequent electrodeposition experiments in order to increase the electrical conductivity of the bath.

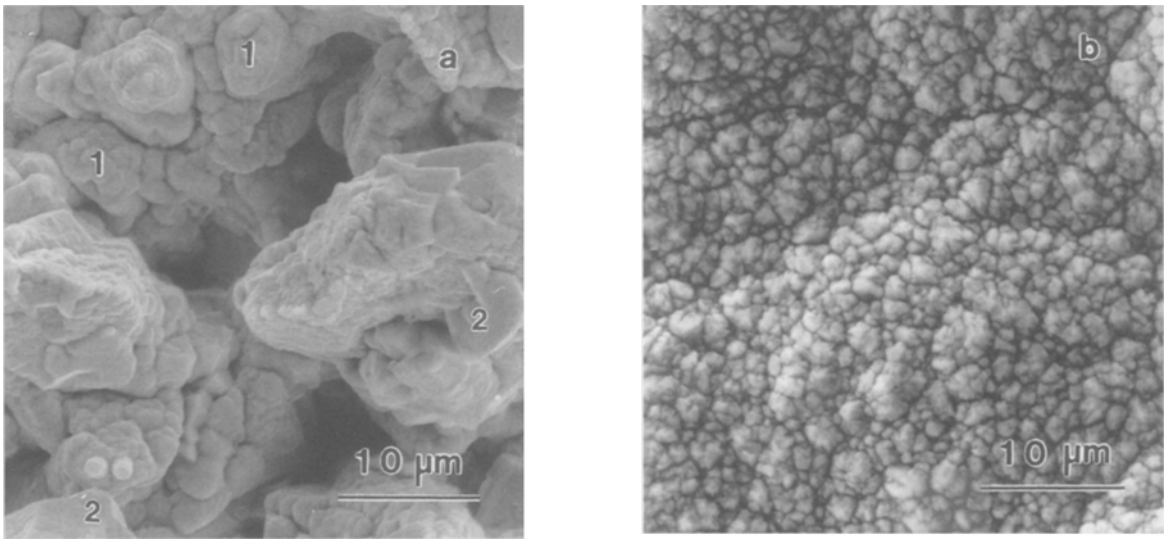

Fig. 4. SEM micrographs of pulse-plated Zn–Ni alloy electrodeposits at $NiCl_2.6H_2O$ concentrations of (a) 50 g dm^{-3} (1 = γ phase and 2 = η phase), and (b) 200 g dm^{-3} .

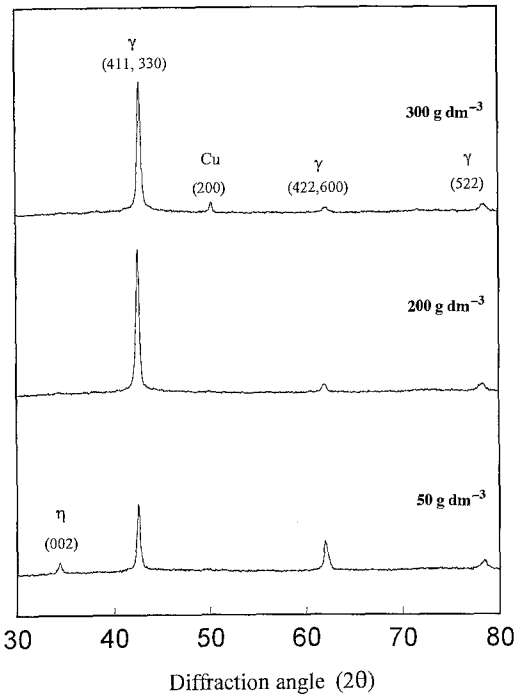

Fig. 5. XRD patterns of Zn–Ni alloy deposits produced at $NiCl_2.6H_2O$ concentrations of 50, 200 and 300 g dm^{-3}.

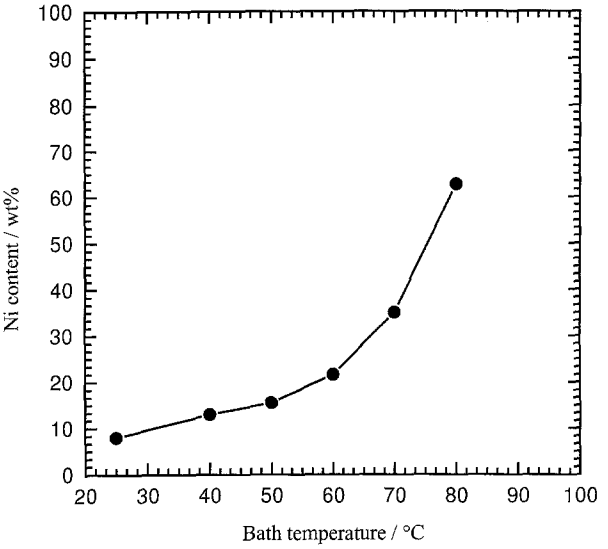

Fig. 6. Change in the deposit Ni content (wt %) as a function of plating bath temperature.

3.1.2. $NiCl_2$ concentration. These series of experiments were performed in order to determine the separate influence of the $NiCl_2$ concentration in the bath on the chemical composition, morphology and phase distribution of the deposit. $NiCl_2.6H_2O$

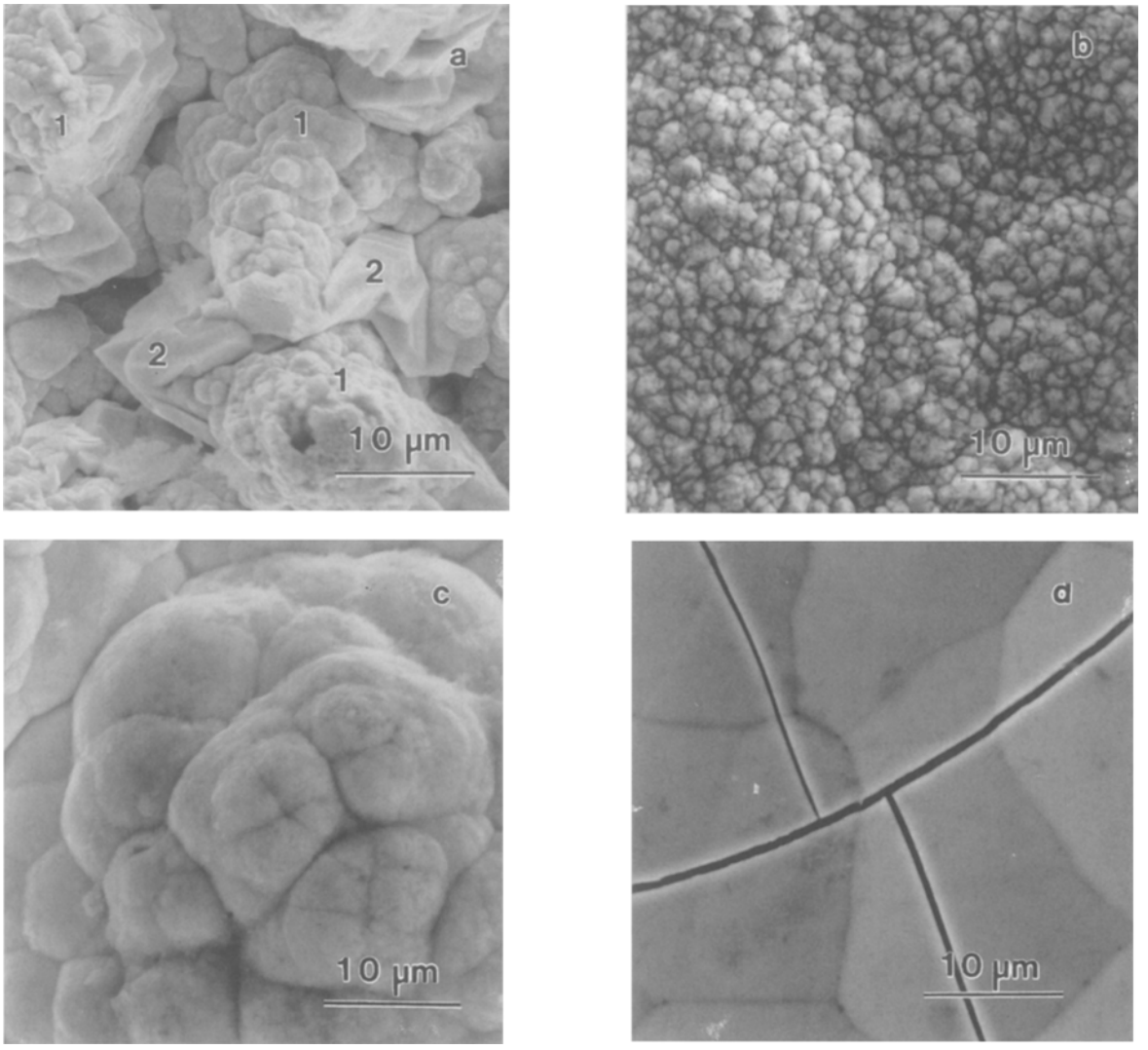

Fig. 7. SEM micrographs showing the effect of temperature on the surface morphology. (a) 25 °C, (b) 40 °C, (c) 70 °C and (d) 80 °C.

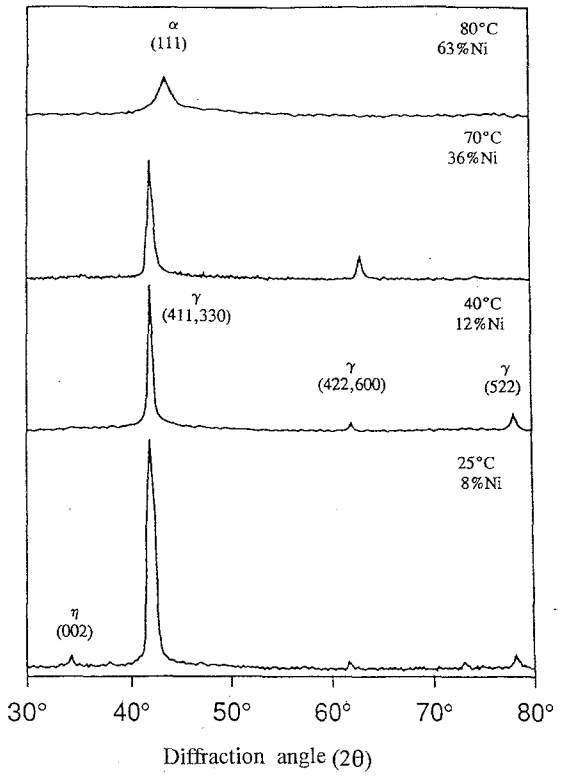

Fig. 8. X-ray diffraction patterns of the Zn–Ni alloys showing the change in phase distribution and preferred crystal orientation as a function of plating temperature.

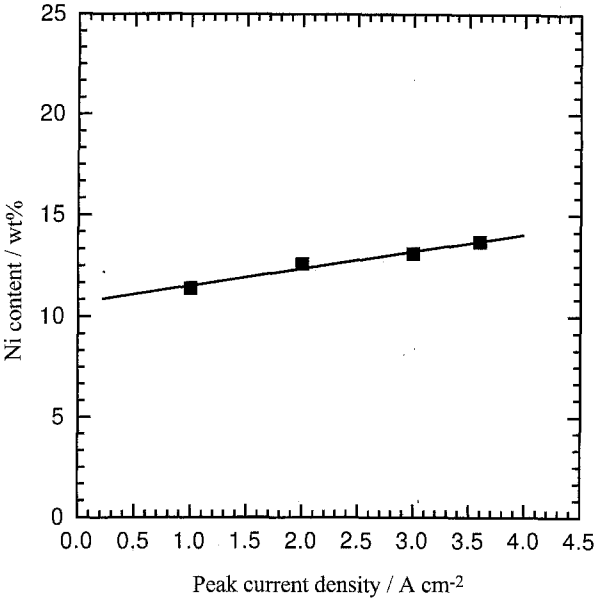

Fig. 9. Change in the deposit Ni content (wt %) as a function of the peak current density.

concentrations in the range of 50 to 300 g dm^{-3} were considered while maintaining the $ZnCl_2$ content in the bath at 200 g dm^{-3}.

Figure 3 shows the effect of varying the $NiCl_2.6H_2O$ concentration in the bath on the chemical composition of the electrodeposit (Ni content). As can be seen, the nickel content of the deposit increased almost linearly from about 7.8 wt % to about 12.5 wt % with increasing $NiCl_2.6H_2O$ concentration in the electrolyte from 50 to 200 g dm^{-3}. Above $NiCl_2.6H_2O$ concentrations of 200 g dm^{-3}, the nickel content in the deposit remained relatively unchanged at about 12–13 wt %. The nickel content in the deposit and in the bath for the various $NiCl_2.6H_2O$ concentrations are listed in Table 5. It is clear from the table that the electrodeposition under these conditions is again of the anomalous type.

These results are consistent with the general trends observed in previous work [23–25] in that increasing the Ni ions in the bath results in an increase in the nickel content in the deposit. It was suggested that the linear relationship observed in the lower range of $NiCl_2.6H_2O$ supports the theory that the reduction of nickel ions is controlled by diffusion. When the $NiCl_2.6H_2O$ increased above 200 g dm^{-3} the process switches to reaction control in which the nickel ion concentration at the cathode surface governs the deposition process. On the other hand the nickel ion concentration in the bulk is critical in controlling the electrodeposition process in the diffusion controlled regime.

The morphology of the deposits produced at $NiCl_2.6H_2O$ concentrations of 50, and 200 g dm^{-3} is shown in Fig. 4. For the deposit produced at 50 g dm^{-3} (Fig. 4(a)) a rough surface morphology is obtained and the structure contains both a fine grained matrix of the γ phase and coarse η phase crystals as revealed by X-ray diffraction (see Fig. 5) and energy dispersive X-ray spectroscopy (EDS) spot analysis. Upon increasing the $NiCl_2.6H_2O$ concentration to 200 g dm^{-3}, the deposit is much smoother and consists entirely of the γ phase with a nodular fine-grained morphology with grain size in the order of 0.5–2 μm (Fig. 4(b)). A further increase in the $NiCl_2.6H_2O$ concentration to 300 g dm^{-3} gave a morphology similar to that of the deposit produced at 200 g dm^{-3} $NiCl_2.6H_2O$ concentration.

Under the experimental conditions tested, $NiCl_2.6H_2O$ concentrations of less than 200 g dm^{-3} would not be suitable for applications where best corrosion resistance is required as at lower concentrations the nickel content of the electrodeposited alloys is out of the range for optimum corrosion resistance (12–14 wt % Ni). In addition it appears more beneficial to use high $NiCl_2.6H_2O$ concentrations ($\geq$200 g dm^{-3}) to produce a consistent deposit composition since even relatively large fluctuations in the $NiCl_2.6H_2O$ concentration in the bath would not alter the deposit composition. The effect of similar fluctuations in the $NiCl_2.6H_2O$ concentrations in the bath at the lower range (50–150 g dm^{-3}) would result in relatively large changes in the chemical composition and phases present in the deposit which, in turn, would require a much closer control of the bath chemistry.

3.2. *Temperature*

The effect of temperature on the characteristics of the deposit was studied in the range of 25 to 80 °C. The other plating variables are as per the standard conditions given in Table 2. Figure 6 shows the change in the chemical composition (Ni content in

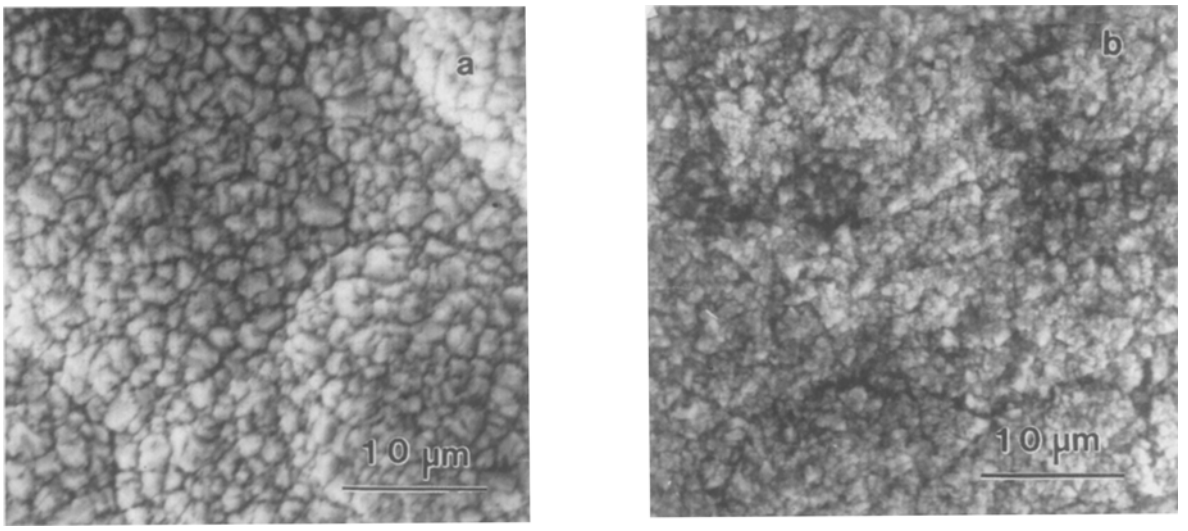

Fig. 10. SEM micrographs of Zn–Ni alloy deposits showing the effect of the peak current density on the surface morphology. (a) 1.0 A cm^{-2}, and (b) 3.6 A cm^{-2}.

wt %) of the deposits as a function of the plating bath temperature. As can be seen the nickel content initially increased slowly as the temperature increased from 25 to 60 °C and then much more rapidly for temperatures between 60 to 80 °C. This behaviour was attributed to the decrease in cathode polarization and enhanced temperature-dependent kinetic parameters [23]. Similar trends were also observed in previous studies on the electrodeposition of the Zn–Ni system for both d.c. [19, 26] and pulse plating [15, 16]. The optimum nickel content for corrosion resistance (12–14 wt % Ni), as reported by Hall [3], was obtained in a temperature range of 30 to 50 °C. The maximum nickel content of 63 wt % was obtained at a temperature of 80 °C.

The effect of temperature on the surface morphology is shown in Fig. 7. For deposits produced at 25 °C, a rough surface morphology is obtained and the structure contains a fine-grained matrix of γ phase and coarse η phase crystals as revealed by XRD (see Fig. 8) and confirmed by EDS spot analysis. Deposits produced at 40 °C are much smoother and the deposit consists entirely of the γ phase with a nodular fine-grained structure morphology with grain size in the range of 0.5 to 2 μm (Fig. 7(b)). At 70 °C, the deposit consists of the γ phase with a massive cauliflower-like morphology with an ultrafine-grained structure with grain size of about 20 nm as determined by XRD line broadening measurements. At the highest temperature tested (80 °C) the deposit consisted of the α phase with a glass-like morphology. In addition this structure shows a relatively large number of microcracks which are an indication of a high degree of brittleness. Line broadening analysis of the

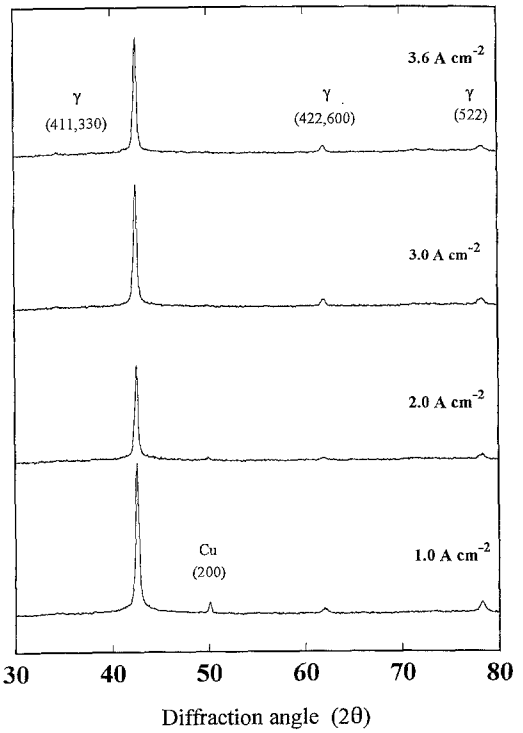

Fig. 11. X-ray diffraction patterns of the Zn–Ni alloys as a function of the peak current density.

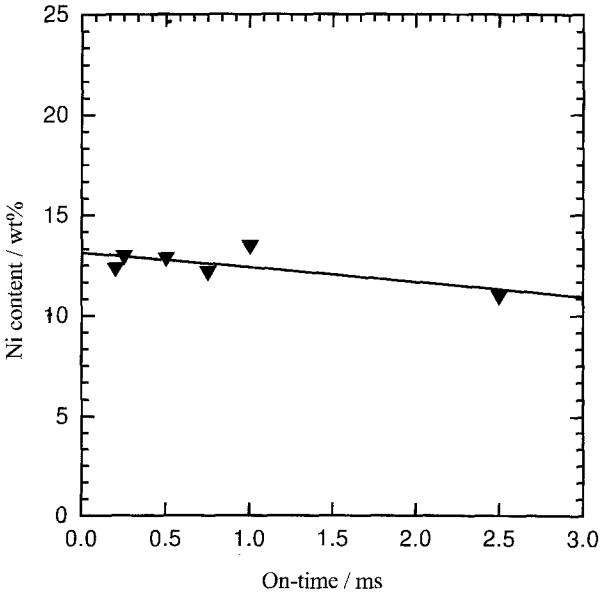

Fig. 12. Change in the deposit Ni content (wt %) as a function of the on-time.

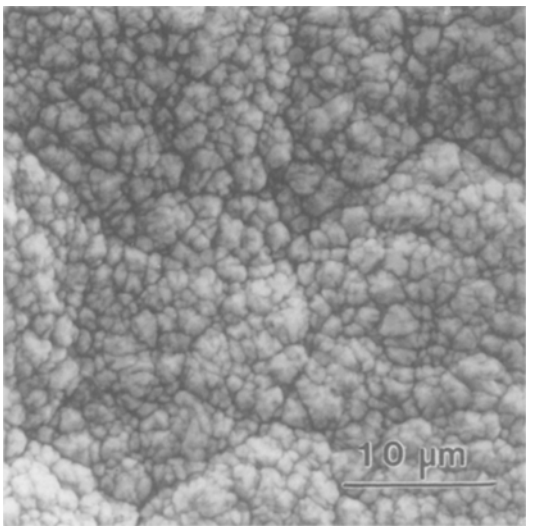

Fig. 13. SEM micrograph of Zn–Ni alloy deposit produced at on-time of 0.75 ms showing surface morphology.

XRD pattern for this deposit indicates that the structure is either nanocrystalline (~2 nm as per Scherrer formula) or amorphous. It should be noted that the transition from nanocrystalline to amorphous in electrodeposited alloys is presently not well understood and that normal X-ray and electron diffraction experiments are not sufficient to unambiguously determine the structure from diffraction peak widths yielding grain sizes of less than 3 nm [27, 28]. Nevertheless the results of the present study are in agreement with a recent study by Fratesi *et al.* [29] who produced amorphous electrodeposits of approximately the same chemical composition using d.c. plating.

The changes in the morphology with temperature observed in this study were mainly due to the variation in the nickel content. Similar results were obtained by Fountoulakis *et al.* [30] in their study of the morphology evolution of d.c. plated Zn–Ni alloy deposits.

It was clarified by Noumi *et al.* [31], using d.c. plating, that bath temperature, along with the other plating variables, have an influence not only on the crystal structure but also on the texture of the Zn–Ni deposits. The deposits produced at 40 °C and 70 °C showed a strong preferred (4 1 1)(3 3 0) orientation. The peak corresponding to the (4 1 1)(3 3 0) reflections is much stronger than expected for a material with random crystal distribution. In other words the deposit has a preferred orientation and grains preferentially align such that either their (4 1 1) or (3 3 0) planes are parallel to the surface of the sample. Unfortunately a θ–2θ diffractometer cannot distinguish between the two planes and the exact texture of the deposit is therefore unknown. Detailed pole figure analysis using a single reflection such as the (5 2 2) plane could solve this problem. Similar results were reported by Fellion *et al.* [23] and Weymeerch *et al.* [26] for d.c. plated Zn–Ni alloys with comparable nickel contents.

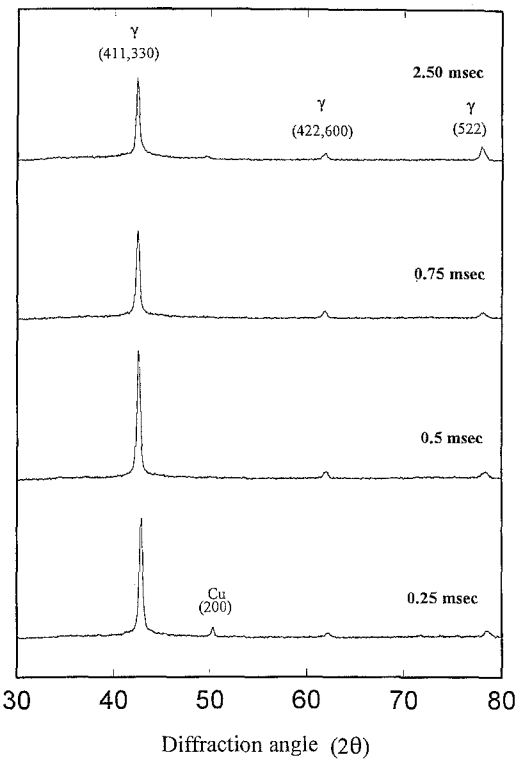

Fig. 14. X-ray diffraction patterns of the Zn–Ni alloys as a function of the on-time.

3.3. *Effect of pulse plating parameters*

3.3.1. Peak current density. The effect of the peak current density (I_p) on the microstructural characteristics of the deposit was tested in the range of 1 to 3.6 A cm^{-2} by adjusting the average current density and keeping the T_{on} and T_{off} constant. An increase in I_p resulted in only a slight increase in the nickel content from 12–14 wt % Ni, as shown in Fig. 9. This is consistent with the results presented by Knodler *et al.* [16] who reported that the nickel content of the deposits is more or less independent of the peak current density at relatively high zinc content in the bath (10 g dm^{-3}). However for baths containing only 5 and 2 g dm^{-3} Zn they found an increase in the nickel content with increasing peak current density.

SEM micrographs showing the effect of I_p on deposit surface morphology are shown in Fig. 10. As can be seen from the figure, an increase in the I_p resulted in considerable grain refinement. For example, the grain size decreased from about 1–2 μm at I_p of 1 A cm^{-2} to a few hundred nanometres at I_p of 3.6 A cm^{-2}. This behaviour is consistent with that reported in the literature for other pulse plated metals [32, 33]. The reduction in grain size is due to the higher over-potential and the accompanied increase in nucleation rate. For the case of alloys, Kim [34] also reported that high I_p results in grain refinement and a corresponding increase in strength for nickel-molybdenum alloy electrodeposits.

These results are also in agreement with the work of Jessen *et al.* [24], who studied the effect of the average current density on the grain size of Zn–Ni alloy produced by d.c. plating technique. They found that

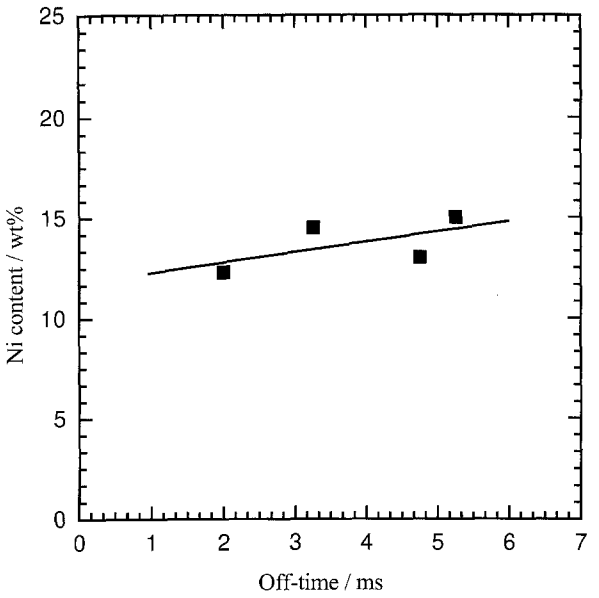

Fig. 15. Change in the deposit Ni content (wt %) as a function of the off-time.

increasing the average current density from 1 to 8 A dm^{-2} resulted in considerable grain refinement.

Figure 11 shows X-ray diffraction patterns of Zn–Ni alloy electrodeposits obtained at I_p of 1, 2, 3, and 3.6 A cm^{-2}. The crystal structure of all deposits was the single γ phase. XRD results also showed that the preferred orientation was always (4 1 1)(3 3 0). It should be noted that the copper peak that appears in one of the spectra (at I_p of 1 A cm^{-2}) is originating from the copper substrate which was partly exposed during the X-ray scan.

3.3.2. Effect of on-time. The effect of the on-time on the microstructural characteristics of the deposit was studied in the range 0.2 to 2.50 ms at a constant temperature of 40 °C. This temperature was selected because the alloy compositions with best corrosion resistance (12–14 wt % Ni) are obtained at this temperature. Figure 12 shows the change of the nickel content (wt %) with T_{on}. It can be seen that T_{on}, in the range tested, had very little effect on the composition; the Ni content remained relatively constant at about 11–14 wt %. A previous study by Knodler *et al.* [16] on the effect of T_{on} on the chemical composition of Zn–Ni alloy deposits also indicated that the nickel content was virtually independent of T_{on}.

The present results also show that T_{on} had insignificant effect on the surface morphology of the deposits as all deposits had faceted fine grained morphology (0.5–2 μm grain size). Figure 13 is a SEM micrograph of a deposit produced at T_{on} of 0.75 ms which illustrates the typical morphology of the deposits obtained for T_{on} range of (0.2 to 2.5 ms). X-ray diffraction patterns for samples plated at $T_{on} = 0.25$, 0.5, 0.75 and 2.50 ms are shown in Fig. 14. The analysis of these patterns show the presence of only the γ phase for all deposits with (4 1 1)(3 3 0) preferred orientation.

3.3.3. Off-time. Figure 15 shows the change of the nickel content in weight per cent as a function of T_{off}. As for the case of T_{on}, T_{off} had little effect on the nickel content of the deposits. The percentage of nickel ranged between 12 and 15 wt %.

The surface morphology of deposits obtained at the different T_{off} values did not change significantly although there is a slight grain refinement as the T_{off} increased from 2.0 ms to 5.25 ms (Fig. 16). This is possibly due to the small increase in the nickel content of the deposit as a result of increasing the T_{off} time.

X-ray diffraction patterns showing the change in texture as a function of T_{off} are presented in Fig. 17. The results show that all of the deposits produced at the various T_{off} had the γ case crystal structure. At relatively small T_{off} (2.0 ms) the deposit had strong (4 1 1)(3 3 0) preferred orientation; with increasing T_{off} values the (4 2 2)(6 0 0) peak intensity increased.

4. Conclusions

Within the ranges considered in this study, the main results of the pulse plating experiments of Zn–Ni

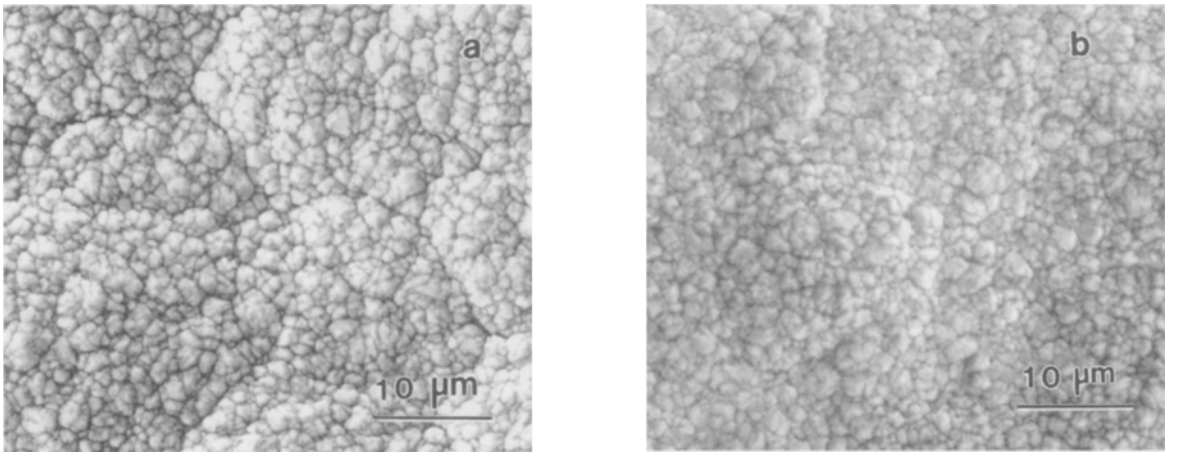

Fig. 16. SEM micrographs of Zn–Ni alloy deposits showing the effect of the off-time on the surface morphology. (a) 4.75 ms and (b) 5.25 ms.

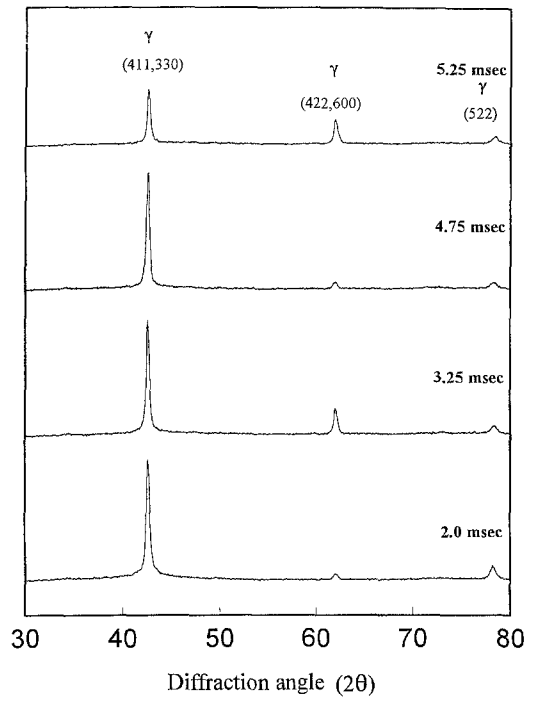

Fig. 17. X-ray diffraction patterns of the Zn–Ni alloys showing the change in preferred crystal orientation as a function of the off-time.

alloys can be summarized as follows:

(i) The effects of bath composition ($ZnCl_2$ and $NiCl_2$ concentration in the bath) support the anomalous codeposition theory presented by Brenner.

(ii) The bath temperature had a very strong influence on the chemical composition of the deposit which in turn had strong effects on phases present, surface morphology and grain size. Within the ranges tested, the best corrosion resistant alloy coatings (14–20 wt % Ni) were obtained at a temperature range of 40 to 50 °C.

(iii) The peak current density was varied between 1.0 and 3.6 A cm^{-2}. It had little effect on the chemical composition and phases present, but considerable effect on the grain size. The grain refinement was attributed to the increase in electrode overpotential resulting from increasing the peak current density.

(iv) The on-time and off-time did not significantly affect the characteristics of the deposit, except for slight grain refinement observed with increasing off-time.

(v) As determined by XRD, only the η, γ and α phases were found in the deposits while other intermediate phases such as β and δ were not observed in any of the deposits produced in this work.

(vi) Grain refinement in the deposits down to the nanocrystalline range can be achieved by increasing the nickel content of the deposit. The peak current density and, to a lesser extent, the off-time have also been shown to refine the grains.

Acknowledgments

The authors of this paper would like to acknowledge the financial support by the Natural Sciences and Engineering Research Council of Canada (NSERC). One of the authors (A.A) was a recipient of Queen's Dean's Awards and Queen's Graduate Awards.

References

[1] S. A. Watson, A Nickel Development Institute Review Series no. 13001, (1988).
[2] F. C. Porter, A. M. Stoneman and R. G. Thilthorp, Inst. Met. Finish. Annual Technical Conference paper, Apr. (1987) 115.
[3] D. E. Hall, *Plat. Surf. Finish.* **70** (1983) 59.
[4] N. Miura, *Trans. Iron and Steel Inst. Japan* **23** (1983) 913.
[5] B. Meuthen, *Plat. Surf. Finish.* **74** (1985) 40.
[6] J. Divisek, P. Malinowski, J. Mergel and H. Schmitz, *Int. J. Hydrogen Energy* **13** (1988) 141.
[7] M. J. De Giz, S. A. Machodo, L. A. Avaco and E. R. Gonzalez, *J. Appl. Electrochem.* **22** (1992) 973.
[8] J. Giridhar and W. J. Wan Ooij, *Surf. Coat. Technol.* **53** (1992) 35.
[9] R. G. Baker and C. A. Holden, *Plat. Surf. Finish.* **72** (1985) 54.
[10] G. F. Hsu, *Plat. Surf. Finish.* **71** (1984) 52.
[11] G. N. K. Ramesh Bapu, G. Devaraj, J. Ayyappa Raju and R. Subramaniam, Industrial Metal Finishing: Proceeding of A Symposium on Industrial Metal Finishing, Karaidudi, India, Central Electrochemical Research Institute, (1985).
[12] B. Arsenault, B. Champagne, P. Lambert and S. Dallaire, IGM88TC-301-668-G, (1988).
[13] J. Ci. Puippe and F. H. Leaman (Eds), 'Theory & Practice of Pulse Plating', AESF Soc. (1986).
[14] C. J. Chen and C. C. Wan, *J. Electrochem. Soc.* **136** (1989) 2850.
[15] I. V. Nenov, Gadshov and K. Pangarov, *Galvanotechnik* **75** (1984) 1107.
[16] V. A. Knodler, C. J. Raub and E. Raub, *Metalloberflacho* **39** (1985) 21.
[17] A. Brenner, 'Electrodeposition of Alloys', vols 1 and 2, Academic Press, New York (1963).
[18] B. D. Cullity, 'Elements of X-ray Diffraction', 2nd edn, Addison-Wesley, (1978).
[19] V. Raman, M. Pushparanam, S. Jayakrishnan and B. A. Shenoi, *Metal Finish.* **81** (1983) 85.
[20] S. R. Rajagapalan, *ibid.* **70** (1972) 52.
[21] T. L. Rama char and S. K. Panikkar, *Electroplat. & Met. Finish.* **13** (1960) 405.
[22] A. M. Alfantazi, A. M. El-Sherik and U. Erb, *Scripta Metall. et Mate.* **30** (1994) 1245.
[23] L. Felloni, R. Fratesi, E. Quadrini and G. Roventi, *J. Appl. Electrochem.* **17** (1987) 574.
[24] C. Q. Jessen, Danish PhD thesis, publication PI.89-10-A/AP.89-10, Technical University of Denmark (1989).
[25] A. Abibis, PhD thesis, University of Aston in Birmingham, UK (1988).
[26] A. Weymeersch, L. Renard, J. J. Conreur, R. Winand, M. Jorda, C. Pellet and C. Mercier, AESF 4th Continous Strip Plating Symposium, Chicago, 1–3 May (1984).
[27] D. Ostrander, MSc thesis, Department of Materials & Metallurgical Engineering, Queen's University, Kingston, Ontario (1993).
[28] G. McMahon and U. Erb, *Microstructural Sci.* **17** (1989) 447.
[29] R. Fratesi and G. Roventi, *J. Appl. Electrochem.* **22** (1992) 657.
[30] S. G. Fountoulakis, R. N. Steinbicker and T. W. Fisher, AES 4th Continous Strip Plating Symposium, Chicago, 1–3 May (1984).
[31] R. Noumi, H. Hagasaki, Y. Foboh and A. Shibuya, SAE Technical Paper No. 820332, presented in Detroit, MI, 22–26 Feb. (1982).
[32] N. Ibl, J. CI. Puippe and H. Augerer, *Surf. Technol.* **6** (1978) 287.
[33] A. El-Sherik, PhD thesis, Department of Materials and Metallurgical Engineering, Queen's University, Kingston, Canada (1993).
[34] W. Kim, PhD thesis, Stevens Institute of Technology, New Jersey (1988).